

Article

# The Role of Neodymium in the Optimization of a Ni/CeO<sub>2</sub> and Ni/CeZrO<sub>2</sub> Methane Dry Reforming Catalyst

Alfonsina Pappacena, Rabil Razzaq, Carla de Leitenburg, Marta Boaro \*  and Alessandro Trovarelli 

Dipartimento Politecnico di Ingegneria e Architettura, Università di Udine, via del Cotonificio 108, 33100 Udine, Italy; alfonsina.pappacena@uniud.it (A.P.); razzaq.rabil@spes.uniud.it (R.R.); carla.deleitenburg@uniud.it (C.d.L.); trovarelli@uniud.it (A.T.)

\* Correspondence: marta.boaro@uniud.it; Tel.: +39-0432-558825

Received: 8 March 2018; Accepted: 28 March 2018; Published: 3 April 2018

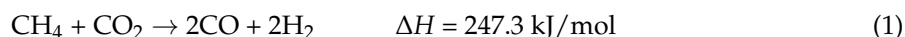


**Abstract:** The development of a sustainable economy based on the use of renewable resources and the reduction of greenhouse gases emissions is an important mandate in modern societies to minimize the global warming. The CO<sub>2</sub>-reforming of methane through a conversion of CO<sub>2</sub> and CH<sub>4</sub> to syngas is a suitable process for this purpose and there is growing interest in the development of new catalysts for this process' application at an industrial scale. This study is the first to investigate methane dry reforming activity of nickel supported on CeO<sub>2</sub> and CeO<sub>2</sub>-ZrO<sub>2</sub> solid solutions doped with neodymium. The supports were synthesized using a surfactant-assisted co-precipitation method and characterized through several analytical techniques to understand the role of synthesis parameters in the distribution of the dopant as well as in the properties of the supports. Co-doping with Zr and Nd resulted in an enhancement of dry reforming activity of ceria due to a higher dispersion of Ni and changes in the strength of basic sites. It was also shown that the addition of Nd helped to mitigate coking issues by increasing the mobility of surface oxygen in ceria and ceria-zirconia oxides and, accordingly, the rate of oxidation of carbonaceous deposits.

**Keywords:** neodymium doping; ceria-zirconia; methane dry reforming

## 1. Introduction

The development of a new economic paradigm based on sustainability through the use of renewable resources is an important objective of modern societies. It requires new technologies as well as upgrading and innovating processes for the conversion and storage of energy [1,2]. Among the traditional methods (partial oxidation and steam reforming) to convert hydrocarbons into valuable products such as hydrogen and syngas, dry reforming of methane (DRM) (Equation 1)) may have potential industrial advantages because it yields syngas with H<sub>2</sub>/CO ratio close to unity which is a preferable feedstock in the production of liquid hydrocarbons and oxygenates [3,4]. Moreover, this process has important environmental implications for the valorization of renewable resources such as biogas (a mixture of CH<sub>4</sub> and CO<sub>2</sub> landfill gases) and for the reduction of greenhouse gas emissions [5]. The reaction is highly endothermic and usually carried out at temperatures higher than 800 °C [6].



In order to lower process costs and to favor its integration with fuel cell technology or other fuel production processes, several studies have recently focused on developing systems and catalysts to decrease the operating temperature in the range of 600–800 °C [7,8]. At these temperatures, in addition

to the DRM, other parallel side reactions are thermodynamically possible (Equations (2)–(4)) causing a decrease in the yield of products and the deactivation of catalysts due to the deposit of coke [9,10].



Although noble metals (Pt, Pd, Ru, Rh) are ideal to overcome these side effects due to their higher selectivity for the DRM reaction [11], from an industrial standpoint, non-noble metals, such as Ni, Co, and Fe, are preferable because they are cheaper and more available [4,7]. Ni is one of the most used and active metals; however, it is prone to coking [12,13]. One strategy to hinder carbon formation and to optimize both CH<sub>4</sub> and CO<sub>2</sub> conversion is to support Ni on different types of supports, such as TiO<sub>2</sub>, SiO<sub>2</sub>, Al<sub>2</sub>O<sub>3</sub>, MgO, CeO<sub>2</sub>, ZrO<sub>2</sub>, and CeO<sub>2</sub>–ZrO<sub>2</sub> [7,8,14]. Both the type of the support and the nature of the metal-support interaction play an important role in the activity and stability of the catalysts. Strong metal-support interactions advantage the dispersion of Ni, increasing activity, while oxygen transfer properties of the support limit the carbon buildup, thus improving stability [6,7].

Ceria-containing catalysts have often shown superior stability with respect to other catalysts owing to the high oxygen storage capacity of ceria [7,8,15,16]. CeO<sub>2</sub> can provide oxygen for both the direct partial oxidation of methane and the oxidation of carbon deposits. Moreover, under reducing conditions, oxygen vacancies and Ce<sup>3+</sup> cations are centers for CO<sub>2</sub> activation by dissociative adsorption [17]. Ceria–Zirconia (CeZr) solid solutions have higher thermal stability and higher oxygen storage capacity with respect to pure ceria [18,19]; however, studies on the use of CeZr on DRM are relatively scarce and sometimes controversial [17,19–22]. Kambolis et al. [23] studied the effect of different compositions on samples prepared by coprecipitation and found that catalysts supported on CeZr are much more active than those supported on pure ceria as a result of a higher number of active sites on the surface of these supports. The highest activity and resistance to coking has been achieved with zirconium rich compositions (Ni/Ce<sub>0.28</sub>Zr<sub>0.72</sub>O<sub>2</sub>). Kumar et al. [21] reported that the addition of zirconium to the ceria lattice led to Ni catalysts with a higher selectivity to H<sub>2</sub> and higher stability towards coking. In several studies, it was pointed out that DRM activity of CeZr-supported catalysts strongly relied on the method of synthesis and on the compositions investigated [20–24]. It was shown that the use of specific surfactants and selected compositions allowed the formation of nanostructured supports, where the formation and control of smaller nickel particles size was easier with positive impact both on the activity and the stability of catalysts [22]. In the literature, it was also reported that the activity of ceria-based catalysts was not straightforwardly related to their bulk oxygen storage capacity. Rather, in order to obtain a more stable and active DRM catalyst, it was important to improve surface oxygen mobility by optimizing the physicochemical surface properties of the support [17].

The addition of rare earth aliovalent ions (RE<sup>3+</sup>) is an effective way to alter the structural and physicochemical properties of ceria and CeZr solid solutions. The doping of CeZr oxides with Pr<sup>3+</sup>, Sm<sup>3+</sup>, La<sup>3+</sup>, and Gd<sup>3+</sup>, caused the formation of oxygen vacancies into the crystal lattice to balance the difference of charge; this generally improved their redox properties, oxygen storage capacity (OSC), and thermal stability [25,26]. Recently, neodymium (Nd<sup>3+</sup>) has been demonstrated to be an effective dopant to stabilize the cubic phase of ceria–zirconia solid solutions in all range of compositions [27] and to improve the catalytic activity of CeZr in the removal of soot and other automotive exhausts [28,29].

To the best of our knowledge, the effect of Nd doping on the methane dry reforming activity of ceria and CeZr materials has not been studied yet, even if neodymium seems to be a promising component to optimize innovative methane dry forming catalysts operating at low temperature (550–750 °C). Good conversions for both CH<sub>4</sub> (62.7%) and CO<sub>2</sub> (82%) at 750 °C, without the formation of relevant carbonaceous deposits, were obtained when Nd<sub>2</sub>O<sub>3</sub> was used as support for Co catalyst [30]. Therefore, this study investigates the preparation of Ni catalysts supported on ceria–zirconia solid solutions (CeZr) and ceria (Ce) doped with neodymium (Nd). The catalysts were characterized by

isothermal N<sub>2</sub> adsorption/desorption (BET and BJH analyses), X-ray diffraction (XRD), temperature programmed reduction/oxidation (TPR/TPO) and desorption of CO<sub>2</sub> (CO<sub>2</sub>-TPD), and finally tested in the DMR reaction with a typical biogas composition. The role of Nd in the activity of these materials has been discussed for further improvements with the aim of optimizing catalytic compositions for the valorisation of biogas from industrial and agricultural wastes.

## 2. Results and Discussion

### 2.1. Effect of the Surfactant

The impact of the surfactant/cation (S/C) molar ratio in the preparation of ceria–zirconia-based supports for methane dry reforming is controversial [21,22]; some authors have claimed that surfactant addition improves textural and redox properties of the support, while others have shown a negative effect as a result of encapsulation phenomena. Therefore, we decided to first study the role of the surfactant in defining the suitable morphology and porosity of CZ supports for the development of Ni active DRM catalysts. This was accomplished using a specific CZ composition Ce<sub>0.80</sub>Zr<sub>0.13</sub>Nd<sub>0.07</sub>O<sub>1.96</sub> prepared by varying the S/C ratio in the range 0–0.98. Figure 1 shows the CH<sub>4</sub> and CO<sub>2</sub> conversion of Ni/Ce<sub>0.80</sub>Zr<sub>0.13</sub>Nd<sub>0.07</sub>O<sub>1.96</sub> for several S/C ratios.

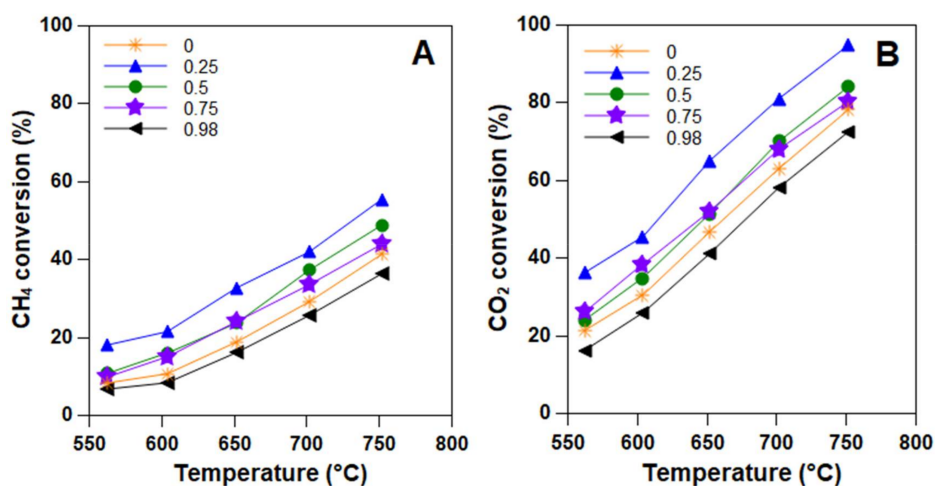
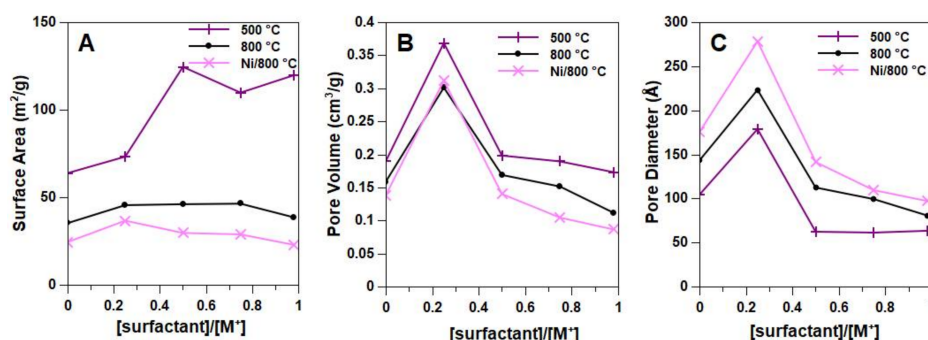


Figure 1. Impact of surfactant/cation (S/C) molar ratio on CH<sub>4</sub> (A) and CO<sub>2</sub> (B) conversion.

Apart from the sample prepared with the highest S/C, both CH<sub>4</sub> and CO<sub>2</sub> conversion were positively affected by the presence of surfactants. However, the relationship between the amount of surfactant and the activity of the catalysts was not linear, and the best performance was obtained with the sample having a S/C molar ratio of 0.25. Figure 2 reports the effect of S/C ratio on the morphological and textural properties of the supports calcined at 500 °C (fresh support) and 800 °C, along with the respective Ni-loaded catalysts. The presence of the surfactant did not affect the sintering process which implies a coarsening of the porosity and a decrease of the surface area of catalysts with temperature and time of calcination. The most active catalyst (S/C = 0.25) showed a higher porosity and pores of larger dimension in comparison with the other samples.

Moreover, Figure 3 shows that the pore size distribution in this catalyst is broad and ranges between 100 and 1000 Å, while the other catalysts are characterized by a bimodal distribution with a high fraction of micropores which decreases after calcination at high temperature. From these results, it is inferred that the higher thermal stability and higher activity observed for the catalyst prepared with a S/C of 0.25 correlated to its peculiar morphology and texture. In the presence of this amount of surfactant ceria–zirconia, crystallites could organize in a refractory structure with a broad mesoporosity which favoured the dispersion of Ni into the pores and its accessibility from the reactant mixture. On the contrary, supports with a large fraction of micropores were not stable and during the calcination

step, micropores collapsed, encapsulating a part of Nickel crystallites. This was also supported by TPR and CO-chemisorption results.



**Figure 2.** Effects of the amount of surfactant on the morphological properties of the ternary CeZrNd<sub>0.07</sub> composition in fresh state (calcined at 500 °C), after calcination at 800 °C, and loaded with Ni followed by calcination at 800 °C: (A) Surface Area; (B) Pore Volume; (C) Pore Diameter.

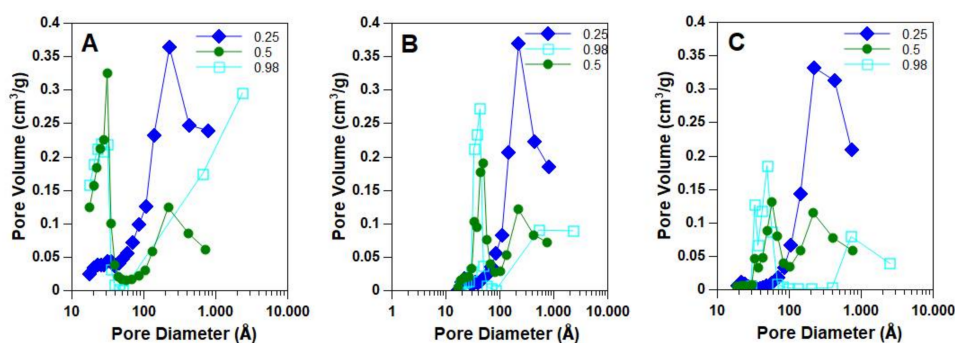


**Figure 3.** Comparison of pore size distribution of samples prepared with a S/C molar ratio of 0.25, 0.5, and of 0.98: (A) after calcination at 500 °C; (B) after calcination at 800 °C; (C) after impregnation of Ni and calcination at 800 °C.

Figure 4 shows TPR profiles of the catalysts prepared with a S/C molar ratio of 0.25 and 0.98, chosen as representative of the entire series. The two profiles were qualitatively similar with two peaks centred at ca. 215 °C and 350 °C, attributable to the reduction of Nickel oxide. The other two peaks at 550 °C and 700 °C was a result of the reaction with support (a detailed comment is given at page 7 and 8) [23].

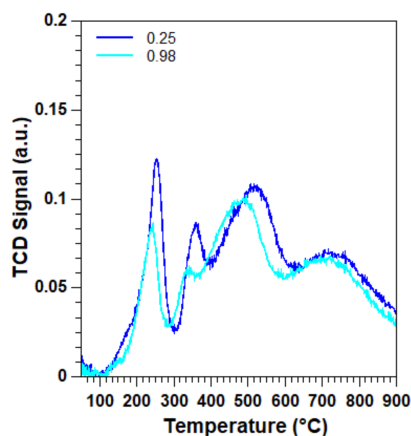


**Figure 4.** TPR of Ni/CeZrNd<sub>0.07</sub> catalyst prepared with two different surfactant/cations molar ratios.

Quantitatively, the hydrogen consumption was 47.8 and 30.4 mL/g for the catalyst with S/C 0.25 and 0.98, respectively. Since the contribution of support to H<sub>2</sub> oxidation was quite similar (26 mL/g vs. and 21 mL/g as calculated from TPR of the support—Figure S1 in Supplementary Materials) the overall difference of H<sub>2</sub> uptake had to be related to a different H<sub>2</sub> accessibility to Nickel. In agreement with this observation, the Ni dispersion resulted in 1.5% for the catalyst prepared with the lower amount of surfactant; however, it was of 0.5% for the catalyst with the larger amount. Taking into account all the above results, further investigation was carried out by considering only samples prepared with a surfactant/cation molar ratio of 0.25.

## 2.2. Morphological, Structural and Redox Characterization of Catalysts

Tables 1 and 2 compare the textural/morphological properties of all the investigated supports and catalysts, respectively. As expected [18], the doping with zirconium contributed to a higher surface area for the supports calcined at 800 °C.

**Table 1.** Morphological and structural properties of supports prepared with a S/C molar ratio of 0.25.

Composition	Name	Temp/Time Calcination (°C/h)	Surface Area (m <sup>2</sup> /g)	Pore Volume (cm <sup>3</sup> /g)	Pore Diameter (Å)	Crystallite Size <sup>1</sup> (Å)
CeO <sub>2</sub>	Ce	800/3	22	0.195	295	298
Ce <sub>0.80</sub> Zr <sub>0.20</sub> O <sub>2</sub>	CeZr	800/3	44	0.374	270	58
Ce <sub>0.80</sub> Zr <sub>0.20</sub> O <sub>2</sub>	CeZr_950	950/3	26	0.313	379	151
Ce <sub>0.80</sub> Nd <sub>0.20</sub> O <sub>1.9</sub>	CeNd <sub>0.2</sub>	800/3	25	0.221	280	178
Ce <sub>0.64</sub> Zr <sub>0.16</sub> Nd <sub>0.2</sub> O <sub>1.9</sub>	CeZrNd <sub>0.2</sub>	800/3	41	0.310	249	77
Ce <sub>0.64</sub> Zr <sub>0.16</sub> Nd <sub>0.2</sub> O <sub>1.9</sub>	CeZrNd <sub>0.2_990</sub>	990/3	22	0.282	384	134
Ce <sub>0.80</sub> Zr <sub>0.13</sub> Nd <sub>0.07</sub> O <sub>1.96</sub>	CeZrNd <sub>0.07</sub>	800/3	45	0.301	223	87
Ce <sub>0.80</sub> Zr <sub>0.13</sub> Nd <sub>0.07</sub> O <sub>1.96</sub>	CeZrNd <sub>0.07_1030</sub>	1030/3	20	0.259	395	170

<sup>1</sup> calculated with Scherrer equation from (111) peak of cubic phase of CeO<sub>2</sub> and of solid solutions.

**Table 2.** Morphological and structural properties of the Ni-catalysts.

Catalysts	Surface Area (m <sup>2</sup> /g)	Pore Volume (cm <sup>3</sup> /g)	Pore Diameter (Å)	Metal Dispersion (%)	Support Crystallite Size <sup>1</sup> (Å)
Ni/Ce	19	0.180	316	0.59	296
Ni/CeZr	34	0.261	255	1.08	100
Ni/CeZr_950	22	0.240	349	1.58	154
Ni/CeNd <sub>0.2</sub>	19	0.196	307	0.58	195
Ni/CeZrNd <sub>0.07</sub>	37	0.311	278	1.56	95
Ni/CeZrNd <sub>0.2</sub>	32	0.311	309	1.28	86
Ni/CeZrNd <sub>0.07_1030</sub>	19	0.243	382	1.93	170
Ni/CeZrNd <sub>0.2_990</sub>	21	0.193	310	1.44	134

<sup>1</sup> calculated with Scherrer equation from (111) peak of cubic phase related to the supports.

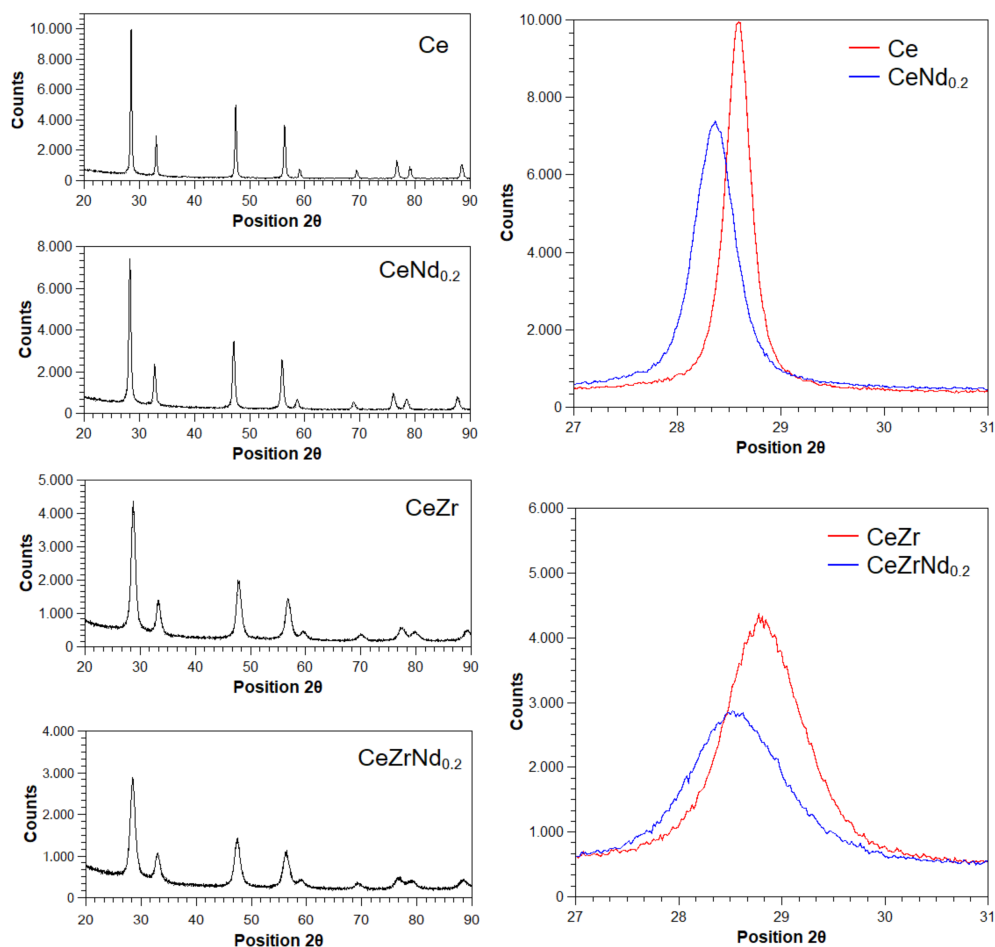
Compared to the standard calcination temperature at 800 °C, some samples were also treated at a higher temperature (990 and 1030 °C) to obtain materials with a reasonable similar surface area range, within 20–25 m<sup>2</sup>/g. It was observed that Nd doping affected the textural properties and crystallinity of CeO<sub>2</sub>, causing a decrease in the dimension of crystallites from 298 Å to 178 Å and an increase in the pore volume. Opposite and less significant effects were observed for CeZr, where the addition of Nd led to a coalescence of crystallites and merging of the pores.

The metal dispersion (see Table 2) was evaluated on reduced samples by CO chemisorption measurements. It was low and likely underestimated as a result of the strong interaction that Ni crystallites may have had with the support. Because of this interaction, the surface electronic density of Ni particles could change, affecting the chemisorption of CO. Moreover, the use of a surfactant during the synthesis of the supports led to the formation of a large fraction of micropores where a part of NiO particles could be encapsulated and was no longer accessible. Clearly, it was the presence of zirconium and not that of neodymium that drove the dispersion of Ni. In fact, CeZr supports were formed by small crystallites rich in surface defects which could stabilize Ni precursors, thus hindering Ni

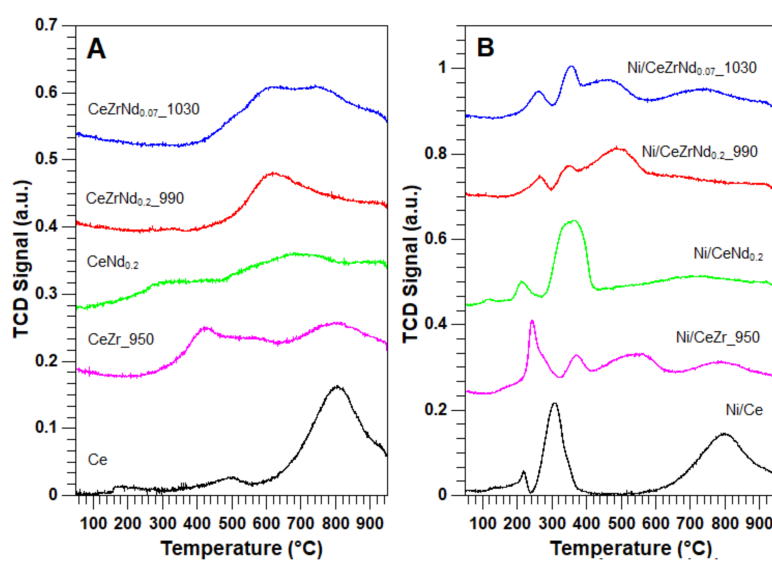
crystallites growth [22]. Moreover, the metal dispersion was higher when CeZr/CeZrNd compositions were calcined above 800 °C. This indicates that CeZr oxides require temperatures above 800 °C to stabilize their morphological and textural properties, i.e., to close the residual microporosity and to obtain large pores suitable for a more homogeneous Ni distribution. The filling of pores with the metal caused a decrease in the surface area of catalysts which depended on both their composition and their thermal history.

Figure 5 shows the XRD profiles of the supports. Ceria and ceria–zirconia solid solution crystallized in a cubic phase which matched respectively with the PDF file of CeO<sub>2</sub> (PDF 34-0394, cell parameter,  $a = 5.4113 \text{ \AA}$ ) and that of Ce<sub>0.75</sub>Zr<sub>0.25</sub>O<sub>2</sub> (PDF 28-0271,  $a = 5.3494 \text{ \AA}$ ). The compositions doped with Nd also showed a cubic structure without any trace of other segregated phases. The XRD of CeZrNd<sub>0.07</sub> (not shown) had the same profile of CeZr solid solution. However, in the XRD profiles of CeNd<sub>0.2</sub> and CeZrNd<sub>0.2</sub>, the peaks were slightly shifted to higher 2θ values with respect to the undoped phases, confirming that Nd entered into the fluorite lattice. XRD profile of CeNd<sub>0.2</sub> and CeZrNd<sub>0.2</sub> matched respectively with that of Ce<sub>0.8</sub>Nd<sub>0.2</sub>O<sub>2-x</sub> (PDF 75-0153,  $a = 5.4480 \text{ \AA}$ ) and Ce<sub>0.5</sub>Zr<sub>0.25</sub>Nd<sub>0.25</sub>O<sub>1.8</sub> (PDF 28-0270,  $a = 5.3690 \text{ \AA}$ ), with compositions close to the nominal one. After impregnation with nickel, all spectra exhibited a very small peak at 2θ = 43.28 degrees (Figure S2 in Supplementary Materials) corresponding to the (200) plane of cubic nickel oxide (PDF 78-0429). The small intensity of this peak suggests that NiO was well dispersed on the supports.

Figure 6 compares the TPR profiles of the supports with the same surface area (A) and the corresponding catalysts (B). It was observed that the undoped materials showed a classical multi-modal profile [22,31]; CeO<sub>2</sub> showed an initial small reduction peak at 500 °C, ascribable to the reduction of the surface, and a second peak at 800 °C, related to the reduction of the bulk Ce<sup>4+</sup> ion. CeZr had a complex reduction pattern with overlapped peaks distinguishable at 400, 500, and 800 °C which related to the nanostructural and compositional surface heterogeneity as well as to the simultaneous reduction of Ce in the surface and in the bulk [18]. Moreover, it is clear that the Nd doping promoted CeNd reduction, which started at a lower temperature and covered a large range of temperatures with two broad bands centered at 300 and 700 °C. Quantitatively, the degree of reduction was higher than that of CeO<sub>2</sub> (see 3rd column on Table 3). The higher degree of CeO<sub>2</sub> reduction observed with the insertion of Nd<sup>3+</sup> into the fluorite lattice was a result of the formation of charge-balancing oxygen vacancies which contributed to a higher mobility of bulk oxygen anions [25]. In the case of CeZr, in which the mobility of bulk oxygen anions was intrinsically higher than that in CeO<sub>2</sub>, the introduction of extra vacancies due to Nd addition had a minor impact. In the CeZrNd compositions, the overall degree of reduction of Ce<sup>4+</sup> to Ce<sup>3+</sup> was lower than that of the binary oxides. These results correlate to previous findings [25,26] and require further investigation to be fully understood. In these oxides, the addition of extra vacancies due to the presence of Nd<sup>3+</sup> may lead to a high vacancies concentration, which, in turn, may aggregate in less mobile clusters. The shift of the reduction onset to higher temperature (Figure 6A) is consistent with this hypothesis. It is also possible that the lower reducibility of ternary compositions are related to the lower content of cerium in the case of CeZrNd<sub>0.2</sub>. In the case of CeZrNd<sub>0.07</sub>, the redox properties could be linked to compositional surface heterogeneity resulting from phase segregation induced by the high temperature (1030 °C) used for the calcination. The reduction profiles of the corresponding Ni catalysts were more complex and generally characterized by the presence of three to four reduction peaks not univocally interpreted in the literature [23]. Generally, the first three peaks at lower temperatures were attributed to the reduction of NiO with different particle sizes and with a strong interaction with the support, while the peak at the highest temperature was related to the reduction of the support. We attributed the peak in the range of 200–260 °C to the reduction of free nanocrystallites of NiO, while the peaks around 300–450 °C were a result of the reduction of larger Ni crystallites and to those Ni species strongly interacting with the support.



**Figure 5.** Comparison of XRD profiles of Ce with CeNd and CeZr with CeZrNd. On the right, details of comparison in the  $2\theta$  range between 24 and 32 degrees, showing the shift of the main peak as a result of the insertion of Nd into the fluorite structure. The lattice parameters of the identified phases are reported in Table S1 (in Supplementary Materials).



**Figure 6.** TPR profiles of (A) supports and of (B) Ni-supported catalysts.

**Table 3.** Quantitative results from TPR profiles of the supports and Ni-supported catalysts.

Samples	Supports H <sub>2</sub> Uptake (mL/g) <sup>a</sup>	Degree of Reduction of Supports <sup>b</sup> (%)	Ni Catalysts H <sub>2</sub> Uptake (mL/g) <sup>c</sup>	Degree of Reduction of Ni Catalysts <sup>b</sup> (%)
Ni/Ce	24.5	38	29.3 (38.0) <sup>d</sup>	45
Ni/CeZr_950	26.5	48	35.7 (40.0)	51
Ni/CeNd <sub>0.2</sub>	30.7	59	38.5 (44.2)	44
Ni/CeZrNd <sub>0.2</sub> _990	18.4	42	28.3 (31.9)	40
Ni/CeZrNd <sub>0.07</sub> _1030	23.5	43	32.2 (37.0)	56

<sup>a</sup> Measured from integration of TPR calibrated profiles of Figure 6A; <sup>b</sup> calculated as the ratio of moles of H<sub>2</sub> consumed and those theoretically consumed for the complete reduction of the reducible species present in a sample, i.e., Ce<sup>4+</sup> moles or the sum of Ce<sup>4+</sup> moles and Ni<sup>2+</sup> moles. The reactions considered in the calculation are 2CeO<sub>2</sub> + H<sub>2</sub> ↔ H<sub>2</sub>O + Ce<sub>2</sub>O<sub>3</sub>; NiO + H<sub>2</sub> ↔ Ni + H<sub>2</sub>O; measured from integration of TPR calibrated profiles of Figure 6B; <sup>d</sup> expected values for a complete reduction of NiO, i.e., (13.5 mL/g) and a partial reduction of support according to the values reported in the second column.

Highlighting the difference among the profiles, we observed that in Ni/CeNd the last peak was less pronounced than in the Ni/Ce catalyst and the peak at 350–450 °C was broader. This is consistent with the occurrence of a spillover mechanism that promotes the bulk reduction at lower temperature. In the case of zirconium-containing oxides, the first peak decreased and shifted at higher temperatures as the amount of Nd increased, suggesting a stronger interaction between NiO and the support in presence of Nd. Quantitatively, we observed the same tendency found for the supports alone (see the fifth column of Table 3). Moreover, it was clear that, for all catalysts, the actual H<sub>2</sub> consumption (third column of Table 3) was lower than the sum of H<sub>2</sub> consumption due to the support reduction (second column of Table 3) and lower than that expected from a complete reduction of NiO (13.5 mL/g of H<sub>2</sub>). The difference between the measured and calculated (indicated in bracket) value followed the rank: CeNd > Ce ≈ CeZr ≈ CeZrNd<sub>0.07</sub> > CeZrNd<sub>0.2</sub>, suggesting that part of NiO may have been either incorporated on the cubic lattice or encapsulated by the support and therefore not completely reduced.

Figure 7 shows the results of CO<sub>2</sub> desorption experiments carried out for the characterization of the basicity of both the supports and the Ni catalysts after their reduction (see materials and methods section). By comparing supports with the same surface area, it was clear that the addition of Nd generally contributed to decrease the basicity of the supports which, when doped, were mainly characterized by the presence of Lewis basic sites of weak strength ( $T < 200$  °C) [32,33]. Considering that Nd<sub>2</sub>O<sub>3</sub> was more basic than the CeO<sub>2</sub> and ZrO<sub>2</sub> [34], this change should have been related to the surface vacancies introduced through the structural doping. Ni-catalysts were characterized by an additional peak at higher temperatures (500–630 °C), attributable to strong basic sites introduced with Ni impregnation and its reduction. Interestingly, the intensity and the position of this peak changed with the composition of the support. The doping of ceria with Zr or Nd shifted the peak position at temperatures lower than 600 °C and, in Nd-doped catalysts, the peak intensity was related to the amount of Nd. In general, a great amount of neodymium contributed to the creation of a higher quantity of mild strength Lewis basic sites ( $T \approx 300$  °C) on the surface of catalysts. The results are consistent with changes in the interaction between metal and ceria supports in the presence of the dopants which leads to different CO<sub>2</sub> adsorption properties for the catalysts.

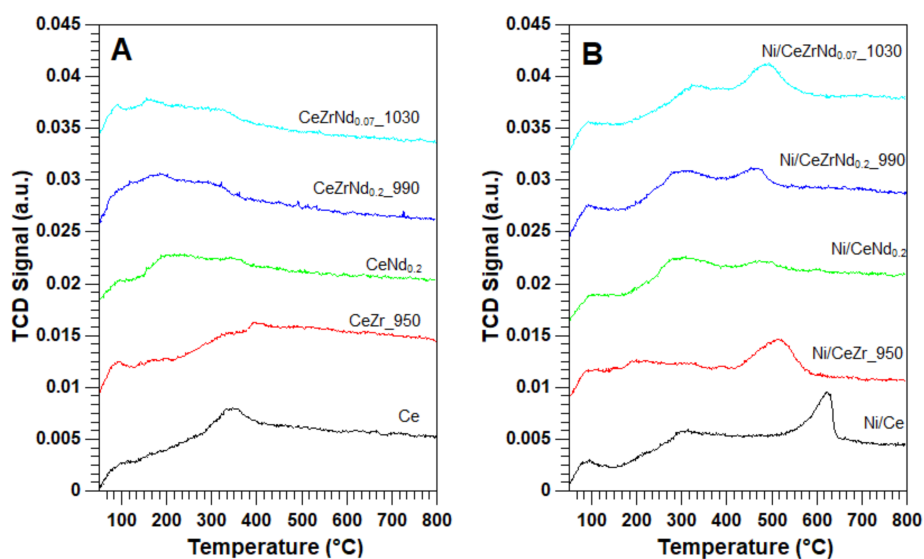


Figure 7. CO<sub>2</sub>-TPD profiles of supports (A) and Ni catalysts (B).

### 2.3. Catalytic Tests

The activity of the catalysts is compared in Figure 8 which shows CH<sub>4</sub> and CO<sub>2</sub> conversion and the H<sub>2</sub>/CO product ratio in the range of temperature from 550 to 750 °C.

All catalysts showed minor activity towards the conversion of methane, which was below the thermodynamic value in the entire range of temperature investigated (Figure 8A). Conversely, the CO<sub>2</sub> conversion was higher and reached a value near to the thermodynamic conversion at 750 °C with the Ni/CeZrNd<sub>0.2</sub>\_990 (Figure 8B). The composition of the supports influenced both CH<sub>4</sub> and CO<sub>2</sub> conversion. In comparison to pure ceria, Zr addition did not affect CH<sub>4</sub> conversion; however, it influenced CO<sub>2</sub> conversion in the range of lower temperatures. On the contrary, Nd doping slightly decreased CH<sub>4</sub> conversion, with little or no influence on CO<sub>2</sub> conversion. On the other hand, the presence of Nd improved both CH<sub>4</sub> and CO<sub>2</sub> conversion of CeZr composition in the entire range of temperatures investigated. This behavior suggests that the dry reforming reaction in these catalysts is ruled by a bi-functional mechanism, in which CO<sub>2</sub> is activated at the metal-support interface and the CH<sub>4</sub> on the surface of metal particles [17]. Since methane conversion is not affected by the dispersion of Ni (see Ni dispersion for Ce and CeZr in Table 2), it was assumed that, for these compositions and in the operating conditions adopted in this study, the rate-determining step was the activation of CO<sub>2</sub> at the perimeters of metal particles. CO<sub>2</sub> was dissociated in CO and mobile oxygen which contributed to oxidize the carbonaceous species (CH<sub>x</sub>) originated by methane dehydrogenation. The presence of Nd seemed to positively affect this mechanism and it was likely responsible for the formation of labile carbonates as intermediates of the reaction (see CO<sub>2</sub>-TPD-results). A mechanism via the reversible formation of an oxy-carbonate as intermediate of reaction was reported for Ni/La<sub>2</sub>O<sub>3</sub> and Ni/La<sub>2</sub>O<sub>3</sub>-ZrO<sub>2</sub> catalysts [35].

The value of the H<sub>2</sub>/CO ratio (Figure 8C) was generally lower than that expected from the stoichiometry of the dry reforming reaction, especially in the case of CeNd-supported catalysts. For the latter composition, the ratio ranged 0.41–0.84; conversely, the ternary CeZrNd compositions showed the highest ratios, reaching values near one at high temperatures. The composition at thermodynamic equilibrium took into account that carbon deposits are mainly formed either via disproportional amounts of CO at low temperatures or via CH<sub>4</sub> cracking at higher temperatures [9,14]. These reactions would contribute to a decreased yield of CO or an increased yield of H<sub>2</sub>. On the other hand, H<sub>2</sub> consumption and CO production could have been affected by the occurrence of the reverse water gas shift reaction in parallel [9].

The above findings demonstrate that the dopants have a significant role in the kinetics of competitive reactions, especially at low temperatures, and that the co-presence of Zr and Nd inhibits the reverse water gas shift reaction (RWGS). CO<sub>2</sub>-TPD results have shown that Nd and Zr contribute to a modification of the distribution of basic sites of CeO<sub>2</sub> and, accordingly, probably the adsorption and activation of CO<sub>2</sub> for the RWGS as well. From the TPR results, it is also clear that co-doping modified the surface redox properties of the supports, decreasing surface oxygen mobility with an advantage for a higher H<sub>2</sub> yield.

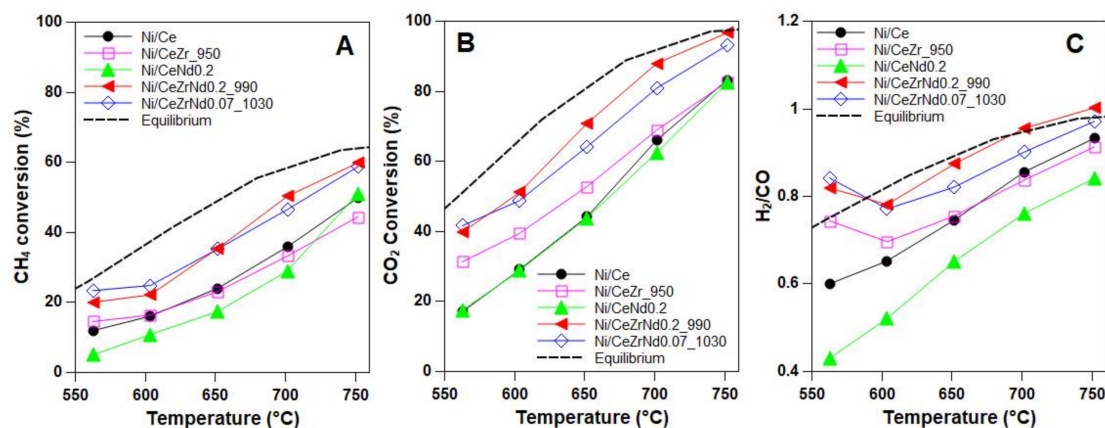


**Figure 8.** Catalytic activity of catalysts investigated: (A) CH<sub>4</sub> conversion, (B) CO<sub>2</sub> conversion and (C) H<sub>2</sub>/CO ratio.

In order to investigate the deactivation processes related to carbon deposition, the catalysts were tested continuously at 650 °C for 8 h, followed by quantification of the amount of carbon formed by thermogravimetric analysis (TGA) under air (Figure 9 and Table 4). The carbon accumulation was proportional to the activity of the catalysts and it occurred mainly in the first hours of testing (a 24 h test leading to an accumulation of 44 wt % of carbon on CeZrNd<sub>0.07\_1030</sub>). The process was probably largely responsible for the deactivation observed in the first three hours of test; it also affected methane conversion more than CO<sub>2</sub> conversion (Figure S3, in Supplementary Materials). Despite the different amounts of carbon deposited, all the resulting catalysts were stabilized with time which suggests that the removal kinetics of carbon from the active sites was rapid.

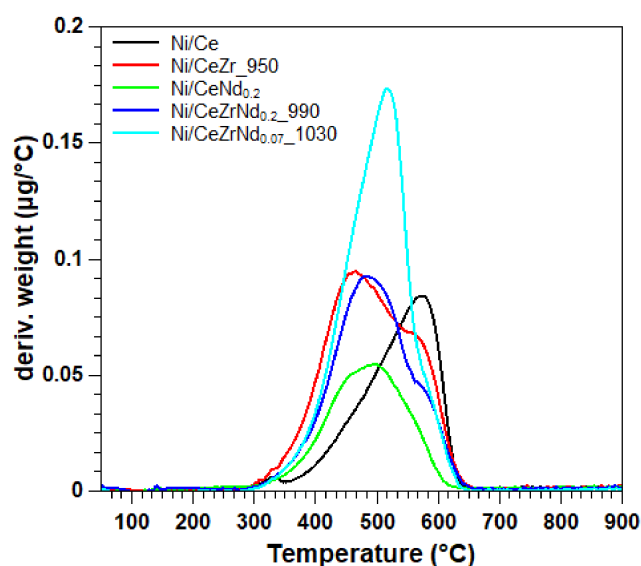


**Figure 9.** Thermogravimetric results of exhausted catalysts after 8 h of testing at 650 °C.

**Table 4.** Amount of carbon formed after durability tests at 650 °C via TGA analysis.

Catalysts	Time on Stream (h)	Carbon %
Ni/Ce	8	22
Ni/CeNd <sub>0.2</sub>	8	17
Ni/CeZr <sub>950</sub>	8	31
Ni/CeZrNd <sub>0.2_990</sub>	8	27
Ni/CeZrNd <sub>0.07_1030</sub>	8	36

Table 4 demonstrates that the samples containing zirconium accumulated more carbon (31–36% vs. 17–22%) and that a great amount of Nd contributed to a decrease in the amount of carbon formed. The beneficial effect of Nd for the removal of carbon also was confirmed in Figure 9 which shows TPO traces of deactivated samples. The profile of Ce-catalyst showed a tailed peak centred at 580 °C, while CeNd showed a broad peak centred at 480 °C. Two overlapping peaks, one at 450 °C and the other at 580 °C, characterize the profile of CeZr. In the latter, the addition of Nd caused the decrease of the second components in favor of the first.

Several studies have categorized the type of carbon deposited on Ni-based catalysts [36]. Ni catalyzes the formation of whiskers and fibers of carbon which can be oxidized above 500 °C [37]. It is inferred that, in the investigated compositions, the presence of Zr and/or of Nd contributed a depression in the formation of graphitic carbon in favor of less refractory forms of carbon [38]. This correlated to a faster kinetics of oxidation as a consequence of doping. The doping with Zr or Nd increased oxygen exchange properties of ceria, providing a more labile lattice oxygen for the oxidation process. On the other hand, a co-doping enhanced the availability of surface oxidant species and the metal-support interaction, making other paths feasible for the removal of carbon.

### 3. Materials and Methods

#### 3.1. Preparation of Catalysts

CeO<sub>2</sub> (Ce), Ce<sub>0.8</sub>Zr<sub>0.2</sub>O<sub>2</sub> (CeZr), Ce<sub>0.8</sub>Nd<sub>0.2</sub>O<sub>1.9</sub> (CeNd<sub>0.2</sub>), Ce<sub>0.64</sub>Zr<sub>0.16</sub>Nd<sub>0.2</sub>O<sub>1.9</sub> (CeZrNd<sub>0.2</sub>), and Ce<sub>0.8</sub>Zr<sub>0.13</sub>Nd<sub>0.07</sub>O<sub>1.9</sub> (CeZrNd<sub>0.07</sub>) were prepared via a surfactant assisted co-precipitation method of synthesis as previously reported [39]. Briefly, the desired stoichiometric amounts of metal salts, such as Ce(NO<sub>3</sub>)<sub>3</sub>·6H<sub>2</sub>O, ZrO(NO<sub>3</sub>)<sub>2</sub> and Nd(NO<sub>3</sub>)<sub>3</sub>·6H<sub>2</sub>O (Treibacher AG, Althofen, Austria), were dissolved in demineralized water to obtain a 0.2 M solution. After that, concentrated H<sub>2</sub>O<sub>2</sub> (35% Sigma-Aldrich, Merck KGaA, Darmstadt, Germany), using a molar ratio H<sub>2</sub>O<sub>2</sub>/total metal ions equal to three, was added to the mixture with continuous stirring for 45 min at room temperature. Next, concentrated ammonium hydroxide (28% Sigma-Aldrich) was added dropwise until the pH of the solution reached a value of 10.5. Finally, lauric acid (LA) (Sigma-Aldrich) was added and the solution was kept under continuous stirring for 4 h. An optimal LA/cations molar ratio of 0.25 was individuated after preliminary experiments in which the ratio varied from 0.25 to 0.98. The solution was then filtered and the filtered cake were dried at 100 °C overnight and then calcined at 500 °C/4 h (fresh samples). Subsequently, samples were calcined at 800 °C/3 h or at higher temperatures, as indicated. About 3.5 wt % of Ni was loaded onto supports by incipient wetness impregnation of Ni(NO<sub>3</sub>)<sub>2</sub>·H<sub>2</sub>O (Sigma-Aldrich) as precursor. After impregnation, the samples were dried at 100 °C overnight and then calcined at 800 °C for 1 h.

#### 3.2. Characterization of Catalysts

Specific surface area and porosity of prepared samples were measured using a Micromeritics surface area and porosity analyzer through N<sub>2</sub> adsorption/desorption isotherms (BET and BJH methods). The samples were previously degassed at 150 °C for 1.5 h to remove moisture and volatile adsorbates.

XRD patterns were obtained to determine the structure of synthesized materials by using a X'Pert X-ray diffractometer (Malvern Panalytical, Almelo, The Netherlands) with a Ni-filtered Cu K $\alpha$  radiation source ( $\lambda = 0.1540598$  nm) equipped with an X'Celerator detector. The operating voltage and current were 40 kV and 40 mA, respectively. X'Pert Highscore software was used for phase analysis and the Scherrer equation with corrected line broadening was used to calculate crystallite size.

A Micromeritics apparatus (Autochem II 2990) (Micromeritics Corporate, Norcross, GA, USA) equipped with a TCD detector was used to perform temperature-programmed H<sub>2</sub> reduction (H<sub>2</sub>-TPR), CO-chemisorption, and temperature-programmed CO<sub>2</sub> desorption (CO<sub>2</sub>-TPD) measurements. (H<sub>2</sub>-TPR) experiments were carried out using a 5% H<sub>2</sub> in N<sub>2</sub> flow, a heating ramp of 10 °C/min up to 950 °C. In order to remove surface carbonates and adsorbed impurities from the surface, all samples were pre-treated in air at 500 °C/1 h and then cooled to room temperature in N<sub>2</sub>. In CO<sub>2</sub>-TPD measurements, the samples were previously reduced at 800 °C/1 h with a 5% H<sub>2</sub>/N<sub>2</sub> flow (35 cc/min) and cooled to room temperature under He flow. CO<sub>2</sub> was left to be adsorbed at 50 °C for 1 h flowing 20% CO<sub>2</sub>/He gas mixture (30 mL/min) through the sample (0.05 mg), and then desorbed with a linear increase of temperatures up to 800 °C after 1 h He flow. The Ni metal dispersion of the catalysts was estimated by CO-chemisorption using a stoichiometry of 1:1 for the calculations [40]. Before the experiment, all samples were reduced in 5% H<sub>2</sub>/N<sub>2</sub> at 800 °C/1 h and cooled to 35 °C under He flow. Then, 5% CO/He was pulsed over the catalyst, recording the pulses until the peaks' area became constant. CO chemisorption experiments were carried out in the same operating conditions also on bare supports and found negligible adsorptions.

### 3.3. Catalytic Tests

The dry reforming tests were conducted at atmospheric pressure in a fixed-bed reactor (i.d. = 4 mm) using 0.08 g of catalyst in powder form (mixed with quarts in a 1:1 ratio). The temperature of the reaction was controlled by a thermocouple placed a few millimeters on the top of the sample. Catalytic experiments were conducted in the temperature range of 550–750 °C on the catalyst previously reduced under hydrogen at 800 °C/1 h. The total volumetric flow was 80 mL/min (with a GHSV of 8000 h<sup>-1</sup>) and CO<sub>2</sub>/CH<sub>4</sub> ratio was fixed at 0.66 to simulate the typical composition of biogas sourced from biogenic waste. Nitrogen was used as internal reference. The composition of the reactor outlet gases mixture (CO, H<sub>2</sub>, CO<sub>2</sub>, and CH<sub>4</sub>) was analyzed with a micro-gas chromatograph (GC, Varian model CP-4900) (Agilent, Santa Clara, CA, USA) equipped with two columns (a molecular sieve and PPQ column) and with a thermal conductivity detector (TCD). The conversion of CH<sub>4</sub> and CO<sub>2</sub> were measured in steady state conditions. The sample was kept at each selected temperature at least 40 min, until the outlet composition resulted constant. The plotted results are calculated averaging the last five chromatographic analyses. The conversions of CO<sub>2</sub> and CH<sub>4</sub> and H<sub>2</sub>/CO ratios were calculated according to the following formulas, where the factor  $\beta = [N_2]_{in}/[N_2]_{out}$  allowed to take into account the changes of flow rate during the reaction.

$$X[CH_4]\% = \{[CH_4]_{in} - ([CH_4]_{out} \times \beta)\} / [CH_4]_{in} \times 100$$

$$X[CO_2]\% = \{[CO_2]_{in} - ([CO_2]_{out} \times \beta)\} / [CO_2]_{in} \times 100$$

$$H_2/CO = [H_2]_{out} / [CO]_{out}$$

Catalyst tolerance to carbon formation was studied at 650 °C. Samples were exposed 8 h at 650 °C to the reactants' mixture and cooled to ambient temperature under inert atmosphere. Subsequently, the amount of formed coke was measured via thermogravimetric analysis (SDT-Q-600 TA instruments, New Castle, DE, USA): 8–10 mg of the spent catalyst, and was heated in air from ambient temperature to 1000 °C at a ramp rate of 10 °C/min, monitoring the loss of weight.

## 4. Conclusions

This study was the first to investigate the activities of Ni/CeO<sub>2</sub> and Ni/Ce<sub>0.8</sub>Zr<sub>0.2</sub>O<sub>2</sub> doped with Nd in the dry reforming reaction of methane. A comparison between Ni/CZ and Ni/CeNd activities showed that, in this process, metal dispersion is a key parameter to be optimized for enhanced performance. It was shown that, by co-doping CeO<sub>2</sub> with Nd and Zr, it was possible to control surface properties of the catalyst such as basicity and surface oxygen mobility. These properties are crucial in the inhibition of processes that contribute to limiting the activity and selectivity of the catalyst, (i.e., the formation of very stable carbonates and the reverse water shift reaction.). Moreover, it was observed that the presence of Nd promoted the surface oxygen mobility of ceria based materials making these compositions more stable to coking deactivation.

**Supplementary Materials:** The following are available online at <http://www.mdpi.com/2304-6740/6/2/39/s1>, Figure S1: TPR of supports prepared with a different surfactant/cations molar ratio, Figure S2: XRD of Ni catalysts; the black dot indicates NiO phase, Figure S3: Endurance test at 650 °C, (A) methane conversion, (B) CO<sub>2</sub> conversion, (C) S/C ratio, Table S1: XRD identified phases.

**Acknowledgments:** Funding from the Italian Ministry of University and Research (MIUR) for the BIO-ITSOFC project (2010KHLKFC 003, PRIN 2010-2011).

**Author Contributions:** Alfonsina Pappacena and Marta Boaro conceived and designed the experiments; Rabil Razzaq performed the experiments and processed the data; Carla de Leitenburg contributed reagents/materials/analysis tools; Marta Boaro wrote the manuscript; Alessandro Trovarelli discussed and revised the manuscript. All the authors contributed to the discussion of data.

**Conflicts of Interest:** The authors declare no conflict of interest.

## References

1. Ghoneim, S.A.; El Salamony, R.A.; El Temtamy, S.A. Review on innovative catalytic reforming of natural gas to syngas. *World J. Eng. Technol.* **2016**, *4*, 116–139. [[CrossRef](#)]
2. Monaco, F.; Lanzini, A.; Santarelli, M. Making synthetic fuels for the road transportation sector via solid oxide electrolysis and catalytic upgrade using recovered carbon dioxide and residual. *J. Clean. Prod.* **2018**, *170*, 160–173. [[CrossRef](#)]
3. Cheekatamarla, P.K.; Finnerty, C.M. Reforming catalysts for hydrogen generation in fuel cell applications. *J. Power Sources* **2006**, *160*, 490–499. [[CrossRef](#)]
4. Frontera, P.; Macario, A.; Candamano, S.; Barberio, M.; Crea, F.; Antonucci, P. CO<sub>2</sub> conversion over supported Ni. *Chem. Eng. Trans.* **2017**, *60*, 229–234. [[CrossRef](#)]
5. Lavoie, J.M. Review on dry reforming of methane, a potentially more environmentally-friendly approach to the increasing natural gas exploitation. *Front. Chem.* **2014**, *2*, 81. [[CrossRef](#)] [[PubMed](#)]
6. Usman, M.; Wan Daud, W.M.A.; Abbas, H.F. Dry reforming of methane: Influence of process parameters—A review. *Renew. Sustain. Energy Rev.* **2015**, *45*, 710–744. [[CrossRef](#)]
7. Wang, Y.; Yao, L.; Wang, S.; Mao, D.; Hu, C. Low-temperature catalytic CO<sub>2</sub> dry reforming of methane on Ni-based catalysis: A review. *Fuel Process. Technol.* **2018**, *169*, 199–206. [[CrossRef](#)]
8. Aramouni, N.A.K.; Touma, J.G.; Tarboush, B.A.; Zeaiter, J.; Ahmad, M.N. Catalyst design for dry reforming of methane: Analysis review. *Renew. Sustain. Energy Rev.* **2018**, *82*, 2570–2585. [[CrossRef](#)]
9. Nikoo, M.K.; Amin, N.A.S. Thermodynamic analysis of carbon dioxide reforming of methane in view of solid carbon formation. *Fuel Process. Technol.* **2011**, *92*, 678–691. [[CrossRef](#)]
10. Shah, Y.T.; Gardner, T.H. Dry Reforming of Hydrocarbon Feedstocks. *Catal. Rev.* **2014**, *5*, 476–536. [[CrossRef](#)]
11. Pakhare, D.; Spivey, J. A review of dry (CO<sub>2</sub>) reforming of methane over noble metal catalysts. *Chem. Soc. Rev.* **2014**, *43*, 7813–7837. [[CrossRef](#)] [[PubMed](#)]
12. Wang, S.; Lu, G.Q.; Millar, G.J. Carbon dioxide reforming of methane to produce synthesis over metal-supported catalysts: State of the art. *Energy Fuels* **1996**, *10*, 896–904. [[CrossRef](#)]
13. Wang, S.; Lu, G.Q. A comprehensive study on carbon dioxide reforming of methane over Ni/ $\gamma$ -Al<sub>2</sub>O<sub>3</sub> catalysts. *Ind. Eng. Chem. Res.* **1999**, *38*, 2615–26253. [[CrossRef](#)]
14. Arora, S.; Prasad, R. An overview on dry reforming of methane: Strategies to reduce carbonaceous deactivation of catalysts. *RSC Adv.* **2016**, *6*, 108668–108688. [[CrossRef](#)]

15. Goula, M.A.; Charisiou, N.D.; Siakavelas, G.; Tzounis, L.; Tsiaoussis, I.; Panagiotopoulou, P.; Goula, G.; Yentekakis, I.V. Syngas production via biogas dry reforming reaction over Ni Supported on zirconia modified with CeO<sub>2</sub> or La<sub>2</sub>O<sub>3</sub> catalysts. *Int. J. Hydrogen Energy* **2017**, *42*, 13724–13740. [[CrossRef](#)]
16. Kumar, P.; Sun, Y.; Idem, O.R. Comparative study of Ni-based mixed oxide catalysts for carbon dioxide reforming of methane. *Energy Fuels* **2008**, *22*, 3575–3582. [[CrossRef](#)]
17. Makri, M.M.; Vasiliades, M.A.; Petalidou, K.C.; Efstathiou, A.M. Effect of support composition on the origin and reactivity of carbon formed during dry reforming of methane over 5 wt % Ni/Ce<sub>1-x</sub>M<sub>x</sub>O<sub>2-δ</sub> (M = Zr<sup>4+</sup>, Pr<sup>3+</sup>) catalysts. *Catal. Today* **2016**, *259*, 150–164. [[CrossRef](#)]
18. Trovarelli, A. Structural and oxygen storage/release properties of CeO<sub>2</sub>-based solid solutions. *Comments Inorg. Chem.* **1999**, *20*, 263–284. [[CrossRef](#)]
19. Nahar, G.; Dupont, V. Hydrogen Production from simple alkane and oxygenated hydrocarbons over ceria–zirconia supported catalysts: Review. *Renew. Sustain. Energy Rev.* **2014**, *32*, 777–796. [[CrossRef](#)]
20. Zeng, S.; Zhang, X.; Fu, X.; Zhang, L.; Su, H.; Hui, P. Co/Ce<sub>x</sub>Zr<sub>1-x</sub>O<sub>2</sub> solid-solution catalysts with cubic fluorite structure for carbon dioxide reforming methane. *Appl. Catal. B Environ.* **2013**, *136–137*, 308–316. [[CrossRef](#)]
21. Kumar, P.; Sun, Y.; Idem, R.O. Nickel-based Ceria, Zirconia and Ceria–Zirconia catalytic systems for low-temperature carbon dioxide reforming of methane. *Energy Fuels* **2007**, *22*, 3113–3123. [[CrossRef](#)]
22. Wolfbeisser, A.; Sophephun, O.; Bernardi, J.; Wittayakun, J.; Föttinger, K.; Rupprechter, G. Methane dry reforming over ceria–zirconia supported Ni catalysts. *Catal. Today* **2016**, *277*, 234–245. [[CrossRef](#)]
23. Kambolis, A.; Matralis, H.; Trovarelli, A.; Papadopoulou, C. Ni/CeO<sub>2</sub>–ZrO<sub>2</sub> catalysts for the dry reforming of methane. *Appl. Catal. A Gen.* **2010**, *377*, 16–26. [[CrossRef](#)]
24. Djinic, P.; Crnivec, G.I.O.; Pintar, A. Biogas to syngas conversion without carbonaceous deposits via the dry reforming reaction using transition metal catalysts. *Catal. Today* **2015**, *253*, 155–162. [[CrossRef](#)]
25. Andriopoulou, C.; Trimpalis, A.; Petalidou, K.C.; Sgoura, C.; Efstathiou, A.M.; Boghosian, S. Structural and redox properties of Ce<sub>1-x</sub>Zr<sub>x</sub>O<sub>2-δ</sub> and Ce<sub>0.80</sub>Zr<sub>0.15</sub>RE<sub>0.05</sub>O<sub>2-δ</sub> (RE: La Nd Pr, Y) solid studies by high temperature in situ Raman spectroscopy. *J. Phys. Chem. C* **2017**, *121*, 7931–7943. [[CrossRef](#)]
26. Mikulova, J.; Rossignol, S.; Gérard, F.; Mesnard, D.; Kappenstein, C.; Duprez, D. Properties of cerium–zirconium mixed oxides partially substituted by neodymium: Comparison with Zr–Ce–Pr–O ternary oxides. *J. Solid State Chem.* **2006**, *179*, 2511–2520. [[CrossRef](#)]
27. Nandi, C.; Grover, V.; Sahu, M.; Krishnan, K.; Guleria, A.; Kaity, S.; Prakash, A.; Tyagi, A.K. Nd<sup>3+</sup> substituted (Zr<sub>1-x</sub>Ce<sub>x</sub>)O<sub>2</sub> (0.0 ≤ X ≤ 1.0) system: Synthesis, structural and thermophysical investigations. *J. Nucl. Mater.* **2016**, *479*, 152–161. [[CrossRef](#)]
28. Wang, Q.; Li, G.; Zhao, B.; Zhou, R. The effect of Nd on the properties of ceria-zirconia solid solution and the catalytic performance of its supported Pd-only three-way catalysts for gasoline engine exhaust reduction. *J. Hazard. Mater.* **2011**, *189*, 150–157. [[CrossRef](#)] [[PubMed](#)]
29. Hernandez-Gimenez, A.M.; dos Santos Xavier, L.P.; Bueno-Lopez, A. Improving ceria–zirconia soot combustion catalysts by neodymium doping. *Appl. Catal. A Gen.* **2013**, *462–463*, 100–106. [[CrossRef](#)]
30. Ayodele, B.V.; Hossain, S.S.; Lam, S.S.; Osazuwa, O.U.; Khan, M.R.; Cheng, C.K. Syngas production from CO<sub>2</sub> reforming of methane over neodymium sesquioxide supported cobalt catalysts. *J. Nat. Gas Sci. Eng.* **2016**, *34*, 873–885. [[CrossRef](#)]
31. Boaro, M.; Vicario, M.; De Leitenburg, C.; Dolcetti, G.; Trovarelli, A. The use of temperature-programmed and dynamic/transient methods in catalysis: Characterization of ceria-based, model three-way catalysts. *Catal. Today* **2003**, *77*, 407–417. [[CrossRef](#)]
32. Binet, C.; Daturi, M.; Lavalley, J.-C. IR study of polycrystalline ceria properties in oxidised and reduced states. *Catal. Today* **1999**, *50*, 207–225. [[CrossRef](#)]
33. Wang, W.; Wang, S.; Ma, X.; Gong, J. Crystal structures, acid-base properties, and reactivity of Ce<sub>x</sub>Zr<sub>1-x</sub>O<sub>2</sub>. *Catal. Today* **2009**, *148*, 323–328. [[CrossRef](#)]
34. Sato, S.; Takahashi, R.; Kobune, M.; Gotoh, H. Basic properties of rare earth oxides. *Appl. Catal. A Gen.* **2009**, *356*, 57–63. [[CrossRef](#)]
35. Sokolov, S.; Kondratenko, E.V.; Pohl, M.-M. Effect of calcination conditions on time on-stream performance of Ni/La<sub>2</sub>O<sub>3</sub>–ZrO<sub>2</sub> in low temperature dry reforming of methane. *Int. J. Hydrogen Energy* **2013**, *38*, 16121–16132. [[CrossRef](#)]

36. Vasiliades, M.A.; Dijnovic, P.; Pintar, A.; Kovac, J.; Efstathious, A.M. The effect of CeO<sub>2</sub>–ZrO<sub>2</sub> structural differences on origin and reactivity of carbon formed during methane dry reforming over NiCo/CeO<sub>2</sub>–ZrO<sub>2</sub> catalysts studied by transient techniques. *Catal. Sci. Technol.* **2017**, *7*, 5422–5434. [[CrossRef](#)]
37. Argyle, M.D.; Bartholomew, C.H. Heterogeneous catalyst deactivation and regeneration: A Review. *Catalysts* **2015**, *5*, 145–269. [[CrossRef](#)]
38. Bartholomew, C.H. Carbon deposition in steam reforming and methanation. *Catal. Rev. Sci. Eng.* **1982**, *24*, 67–112. [[CrossRef](#)]
39. Pappacena, A.; Schermanz, K.; Sagar, A.; Aneggi, E.; Trovarelli, A. Development of a modified co-precipitation route for thermally resistant, high surface area ceria–zirconia based solid solutions. *Stud. Surf. Sci. Catal.* **2010**, *175*, 835–838. [[CrossRef](#)]
40. Brooks, C.S.; Christopher, G.L.M. Measurement of the state of metal dispersion on supported Nickel catalysis by gas chemisorption. *J. Catal.* **1968**, *10*, 211–223. [[CrossRef](#)]



© 2018 by the authors. Licensee MDPI, Basel, Switzerland. This article is an open access article distributed under the terms and conditions of the Creative Commons Attribution (CC BY) license (<http://creativecommons.org/licenses/by/4.0/>).